Desalination and Water Treatment
www.deswater.com

doi: 10.5004/dwt.2021.27308

228 (2021) 376–388
July

Simultaneous adsorption of methylparaben and propylparaben dyes from aqueous solution using synthesized *Albizia lebbeck* leaves-capped silver nanoparticles

Fatemah Maghami[a], Maryam Abrishamkar[b,*], Bijan Mombeni Goodajdar[a,*], Mina Hossieni[a]

[a]*Department of Chemistry, Omidiyeh Branch, Islamic Azad University, Omidiyeh, Iran, emails: bmombini@gmail.com (B.M. Goodajdar), fatemeh.maghami.2015@gmail.com (F. Maghami), Mina.hosseiny@gmail.com (M. Hossieni)*
[b]*Department of Chemistry, Ahvaz Branch, Islamic Azad University, Ahvaz, Iran, email: abrishamkar.maryam2020@gmail.com*

Received 16 September 2020; Accepted 8 April 2021

ABSTRACT

The *Albizia lebbeck* leaves-capped silver nanoparticles (ALLC AgNPs) were synthesized, and their applicability for dyes eliminating from aqueous media have been investigated. Identical techniques, including scanning electron microscopy, Fourier transform infrared spectroscopy, and X-ray diffraction analysis, utilized to characterize these novel materials. The ALLC AgNPs were found available, suitable, and bargain-counter adsorbents for the proper removal of methylparaben (MP) and propylparaben (PP) dyes from aqueous media. By examining the effect of different parameters, it was found that the percentage of adsorption and the initial concentrations of MP and PP dyes were inversely related, while the percentage of adsorption and adsorbent dose were directly related. It was shown that the maximum adsorption of MP and PP dyes and their removal by adsorbent was at pH 7.0. The adsorbent dosage of 50 mg in pH 7 has been considered the optimum values for adsorption of MP and PP dyes with a concentration of 10 mg/L onto ALLC AgNPs. The Langmuir model was better at describing equilibrium data than other models. Enthalpy ($\Delta H°$), entropy ($\Delta S°$), and free energy ($\Delta G°$) as thermodynamic parameters of adsorption were determined using isotherms. The fact that the adsorption process was endothermic was well reflected by negative values ($\Delta G°$, $\Delta H°$, and $\Delta S°$), which alone indicated the tendency to synthesize ALLC AgNPs to remove MP and PP dyes. The maximum monolayer coverage capacity (q_{max}) was 6.7 mg/g for MP and 8.5 mg/g for PP at desired conditions.

Keywords: Adsorption; Paraben dyes, Isotherms, *Albizia lebbeck* leaves-capped silver nanoparticles, Thermodynamic

1. Introduction

The severity of water pollution has resulted from the economic development adopted by humans all over the world. The textile industry consumes huge quantities of water and generates enormous impurities including dyes, detergents, additives, suspended solids, aldehydes, heavy metals, non-biodegradable matters, and insoluble substances [1]. According to recent reports, more than one million dyes are commercially available with an annual production of over 7×10^5 tons. The textile industry consumes approximately 1×10^4 tons of dyes annually and discharges nearly 100 ton/y into wastewater [1,2]. Industrial wastewater from textile, paper, rubber, plastic, leather, cosmetic, food and drug industries contains dyes and pigments that are hazardous and can cause allergic dermatitis, skin irritation, cancer, and mutation in living organisms [2]. In addition, their inhalation can affect the respiratory tract with symptoms of rapid

* Corresponding author.

or difficult breathing; while their oral ingestion can affect the gastrointestinal tract with symptoms of burning sensation, nausea, vomiting, hyperhidrosis disorder, cognitive impairment disorder, micturition disorder, and methemoglobinemia syndrome [3].

Parabens as a series of p-hydroxybenzoate acids are synthetic chemicals that have been utilized as preservatives and antimicrobials in various products, especially personal care products, pharmaceuticals, food, beverages, and industrial products [4,5]. Four widely used preservatives in daily use products including butylparaben, ethylparaben, methylparaben (MP), and propylparaben (PP) are used either individually or in combination [6]. However, previous studies have been indicated that continued exposure to parabens, even at low concentrations, can cause alterations to the endocrine system of vertebrates. Recently, the evidence of parabens that have been identified in human breast tumor tissues has been presented, and they were also found as the cause of male infertility as a result of testis mitochondrial dysfunctions [7,8]. In some reports, it was declared that parabens could stimulate the growth of some types of breast cancer [9] if applied for a long time. Also, in several published studies, some male reproductive disorders have been associated with high paraben concentrations [10]. Generally, parabens found their path to municipal sewage systems. Eliminating parabens by some wastewater treatment technologies is possible [11]. However, small amounts of parabens (at a low level of ng/L) have been spotted in river water samples [12]. Also, the appearance of parabens in samples of soils and sediments has been considered by environmentalists [13].

Adsorption as an excellent and uncomplicated technique is better than other conventional protocols, namely ion exchange, chemical coagulation, electrolysis, and biological treatments in eliminating harmful and toxic contaminations. Absorption deserves its popularity due to its advantages such as uncomplicated and mild operating conditions, higher efficiency, and lower waste [14].

Also, the effectiveness of adsorption techniques in the removal of contaminations has been confirmed [15]. The chemical and physical attributes of an adsorbent characterize the efficacy of an adsorption process. Valuable properties are considered as follows: having high absorption capacity, availability, and recycling as well as being economical. It has been tried to eliminate specified organic materials from water samples by applying various potential adsorbents in recent years. In this regard, metallic nanoparticles have been widely considered as a unique adsorbent thanks to their small diffusion resistance, high adsorption capacity, and large surface area. For instance, their application in the separation and removal of chemical species like dyes, environmental pollutants, gases, and metals has been proved to be successful [15].

Silver nanoparticles (AgNPs) have various applications and are used in different areas, from medical devices to electronic devices or paintings and coatings, soaps, and detergents of various sizes and shapes [16]. Specifically, the application of colorimetric sensors equipped with AgNPs has attracted a lot of attention due to their distinctive optical properties and localized surface plasmon resonance absorption [17]. Additionally, the confirmed antimicrobial characteristics of Ag^+ ions leads to the extensive application of AgNPs. Therefore, AgNPs have been utilized in the pharmaceutical industry, nanomedicine, biomedical engineering, and biosensing, thanks to their exclusive properties [18]. The functionalization of surface and AgNPs stabilization are important in metal ions sensing [19]. Therefore, in strengthening AgNPs in the mentioned applications, it is essential to know their physical, optical, and chemical properties. From this point of view, in their synthesis, attention to the following details of materials is critical: (1) surface properties, (2) size distribution, (3) appearance morphology, (4) particle composition, and (5) dissolution rate.

In this current study, AgNPs were synthesized and modified with ALLC. The synthesized AgNPs were applied as unique adsorbents for the removal of MP and PP. The characterization of synthesized *Albizia lebbeck* leaves-capped silver nanoparticles (ALLC AgNPs) was investigated by Fourier transform infrared spectroscopy (FT-IR), scanning electron microscopy (SEM), and X-ray diffraction (XRD) analyses. In the process of MP and PP dyes removal, the effects of essential variables, including solution pH, contact time, adsorbent dosage, and initial concentration of dyes, as well as the dye removal percentage as a response, were investigated and optimized [6]. Also, adsorption equilibrium isotherms and adsorption kinetics of MP and PP dyes removal onto ALLC AgNPs based on the mathematical relationships were studied. The effective success of the ALLC AgNPs in removing the dyes was proven.

2. Experimental section

2.1. Equipment

The morphology of the sample was evaluated in detail using a SEM (KYKY-EM3200, China) by applying an accelerating voltage of 26 kV. UV-Visible spectra data were obtained through UV/Vis spectrometer (Perkin-Elmer, Lambda 25). FT-IR spectrometer (JASCO, FT/IR 420) was used for FT-IR analysis. On a JEOL 3010, transmission electron microscopy images of nanoparticles were registered. For measuring the pH, Metrohm pH/Ion meter model 781 (Switzerland) was employed. Throughout the night, the laboratory glassware was left in 10% nitric acid.

2.2. Chemicals

All chemicals such as MP and PP dyes, silver nitrate ($AgNO_3$), sodium hydroxide (NaOH) and hydrochloric acid (HCl) in the highest available pure form were provided from Merck Co., (Darmstadt, Germany). To prepare the stock solutions in this study, double distilled water (DDW) was used. By dissolving 10 mg of solid dye in 100 mL DDW, the stock solutions of MP and PP dyes (10 mg/L) were prepared, which were diluted daily to prepare working solutions.

2.3. Synthesis of ALLC AgNPs

Preparation of ALLC AgNPs was performed by reduction of $AgNO_3$ by *Albizia lebbeck* Leaves as a reducing and

modifying agent. Briefly, 10.0 mL of *Albizia lebbeck* Leaves (0.1 mM) solution was added to 90.0 mL of $AgNO_3$ (0.1 mM) solution in a reaction flask while the solution was vigorously stirred. After stirring the obtained solution for 1 h at ambient temperature, the color of the colloidal solution changed from dark to bright yellow that confirmed the formation of ALLC AgNPs. The ALLC AgNPs solution was stable for several weeks.

2.4. Adsorption of MP and PP dyes onto ALLC AgNPs

A batch process using ALLC AgNPs was applied for binary adsorption of MP and PP dyes. A tubular glass container was utilized for all of the experiments. Firstly, an adequate amount of adsorbent (50 mg) was added to the solution containing 10 mg/L of two dyes (MP and PP), while the pH was adjusted to 7.0. Next, the glass container was dipped in the bath at ambient temperature for 60 min and then it was centrifuged. The amounts of non-adsorbed dyes were designated with a UV-Vis analysis at a wavelength of 680 nm.

2.5. Batch adsorption process of dyes

Batch adsorption tests were performed to define the MP and PP dye adsorption isotherms on ALLC AgNPs and determine its kinetic properties. First, a 100 mL solution containing 10 mg/L of MP and PP dyes was prepared.

After adjusting the pH of the solution with 0.01 M of HCl and NaOH solutions, the solution was divided into samples of 50 mL in flasks. Then, 10 mg/L of adsorbent was added to each sample, separately. The effects of significant parameters included pH, contact time, adsorbent dosage, and temperature, were studied on the adsorptive removal of two parabens onto ALLC AgNPs. Standard solutions were prepared by diluting stock solutions (10 mg/L parabens mixture (1:1 of MP:PP). Their pH was adjusted to the required values (4.0–10.0), and suitable quantities of the adsorbent (10–60 mg) were added. These solutions were agitated at 180 rpm speed on an orbital shaker at a controlled temperature of 25°C. This mixture was then sonicated for about 5–80 min. ALLC AgNPs were filtered from aqueous solution through a No. 42 of Whatman filter paper, and the concentrations of MP and PP dyes in the solution were measured at 680 nm (Fig. 1). The calculation of the equilibrium adsorbed dyes quantities (q_e, mg/g) was done employing the following equation:

$$\%\text{Removal} = \frac{\left(C_0 - C_t\right)}{C_0} \times 100 \tag{1}$$

where C_0 and C_t refer to the initial concentration of dyes (mg/L) and their concentrations at any time (mg/L), respectively.

$$q_e = \frac{\left(C_0 - C_e\right)V}{W} \tag{2}$$

In the above equation, q_e, C_0, C_e, V, and W refer to adsorption capacity (mg/g), the primary concentrations of dyes (mg/mL), the equilibrium concentrations of dyes (mg/mL), the volume of the aqueous phase (mL), and the weight of the adsorbent (g), respectively.

3. Results and discussion

3.1. Characterization of adsorbent

3.1.1. Brunauer–Emmett–Teller analysis of ALLC AgNPs

The nitrogen adsorption–desorption isotherm of a 77 K onto ALLC AgNPs is presented in Fig. 2. This isotherm is in accordance with the classical type III isotherm of IUPAC classification [20,21]. The porosity and chemical reactivity of functional groups of the surface control the adsorption capacity of ALLC AgNPs was also investigated. Comprehensive knowledge of the surface functional groups would provide an overview of the adsorption potentiality of the ALLC AgNPs (Table 1).

3.1.2. XRD analysis

The XRD pattern of the ALLC AgNPs (Fig. 3) represents peaks at 45.0 (111), 51.5 (200), 72.2 (220), and 54.4 (231), which are related to reflections and diffraction pattern of crystal

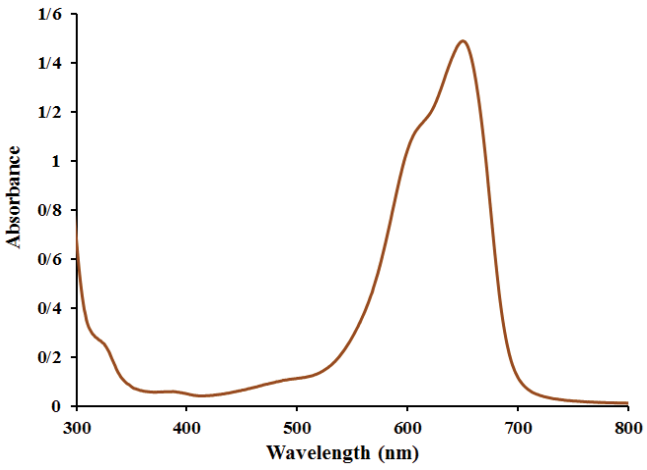

Fig. 1. Sorption spectra of adsorption of MP and PP dyes by ALLC AgNPs.

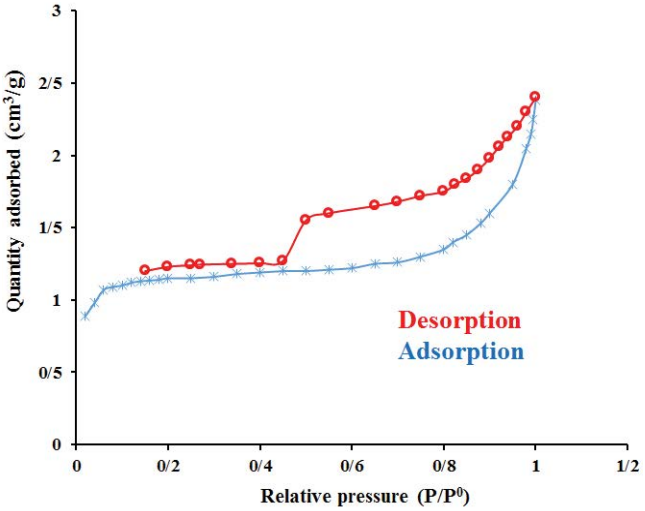

Fig. 2. N_2 adsorption–desorption isotherms of ALLC AgNPs.

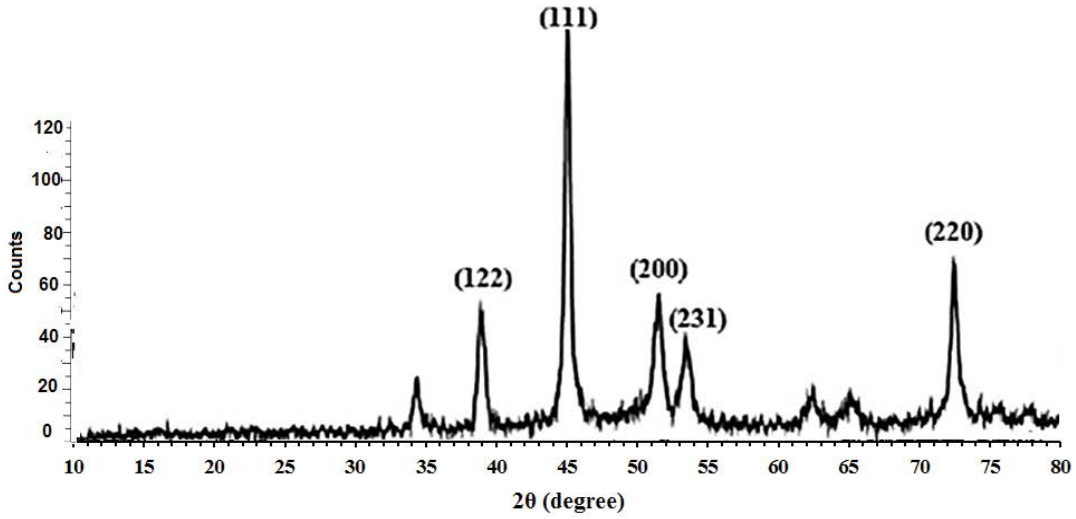

Fig. 3. XRD of the prepared ALLC AgNPs.

[22]. As can be seen, the entirely crystalline structure is confirmed, while the high intensity of peak at 45.0 (111) indicates the presence of low quantities of substances in an amorphous condition.

3.1.3. FT-IR analysis

In the FT-IR spectrum of ALLC AgNPs, the absorption peaks observed at 3,451 cm^{-1} indicates the O–H group's attendance, which is related to the alcoholic or phenolic groups (Fig. 4). The peaks appeared at 3,101 cm^{-1} show the attendance of C–H groups. Similarly, the peaks observed at 2,158 cm^{-1} show the attendance of the C=O group. The peak appeared at 776.8 cm^{-1}, corresponding to the Ag–O group of the ALLC AgNPs. Due to the activation of heavy metals through complex formation or electrostatic adsorption between metal ions and oxygen-containing functional groups, the study and evaluation of functional groups are necessary [23].

3.1.4. Energy-dispersive X-ray spectroscopy and X-ray fluorescence analysis

Energy-dispersive X-ray spectroscopy (EDX) spectrum of the prepared *Albizia lebbeck* leaves (Fig. 5a), and EDX spectrum recorded from a film after the formation of silver nanoparticles (Fig. 5b) [24]. The chemical analysis of preparation was done using X-ray fluorescence (XRF) technique, and its results are presented in Table 2. The analysis results proved the presence of (Ca, K and Mg ions) in the structure of the prepared adsorbent, which can improve its adsorption capacity [25].

X-ray fluorescence spectrometry (XRF) is a relatively effective quantitative technique to determine the elemental composition of any material, with trace element abundances at the ppm level. Correspond lines of X-ray emitted from Si, O, and C elements were observed. *Albizia lebbeck* leaves composition percentage of elements calculation results listed in Table 2.

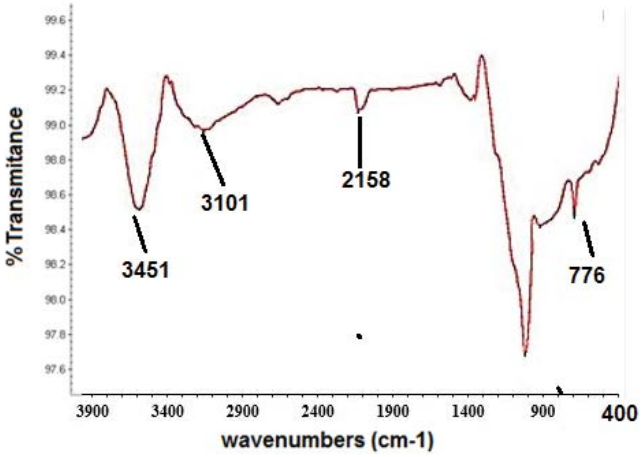

Fig. 4. (a) FT-IR spectra of the prepared *Albizia lebbeck* leaves extracted and (b) FT-IR spectra of the prepared ALLC AgNPs.

Table 1
Brunauer–Emmett–Teller surface area analysis of the adsorbents

	Samples	
	ALLC	ALLC AgNPs
Surface area (m^2/g)	81.45	97.85

3.1.5. Surface morphology

The morphology of nanoparticles was studied using SEM that is shown in Fig. 6. ALLC AgNPs depicted the be homogeneous, smooth, regular, and almost equal size distribution as individual particles and aggregates.

3.1.6. Point of zero charge

Qualitative assessment of the type of interaction (attraction or interaction) between sorption ALLC AgNPs and dyes will be possible if we know the type of charges on

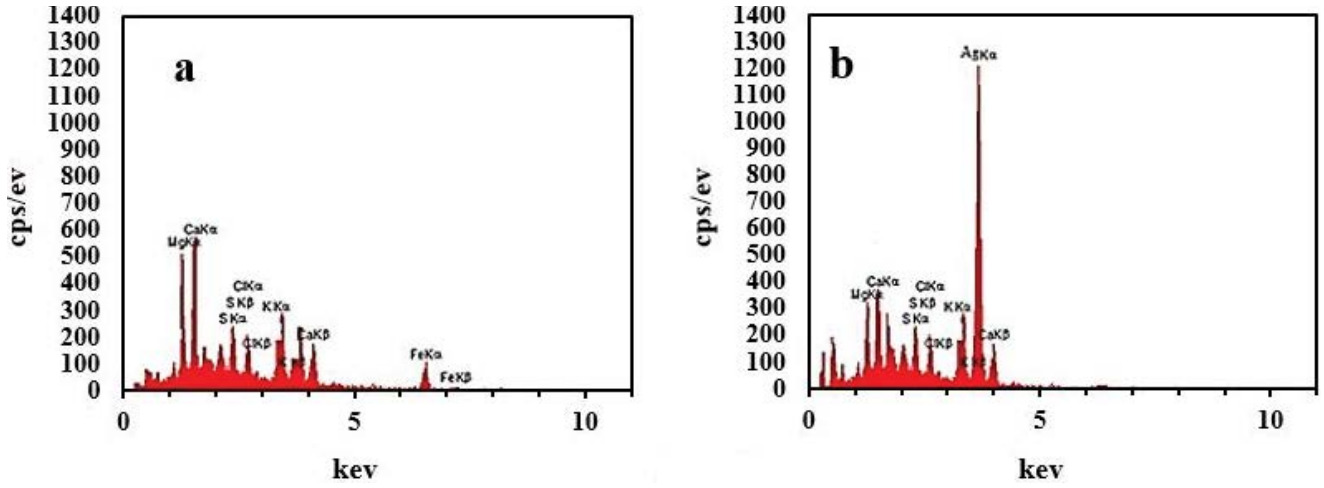

Fig. 5. (a) EDX transmittance spectrum of the prepared *Albizia lebbeck* leaves and (b) EDX spectrum recorded from a film, after the formation of silver nanoparticles.

Table 2
Results of X-ray fluorescence (XRF) analysis of the prepared *Albizia lebbeck* leaves

Elt	Line	Int	Error	K	Kr	W%	A%	ZAF	Pk/Bg	Class	LConf	HConf
C	Ka	225.9	18.0269	0.4893	0.2187	52.33	66.26	0.4178	144.50	A	51.30	53.37
O	Ka	90.2	18.0269	0.0973	0.0435	25.34	24.09	0.1715	32.29	A	24.55	26.14
Mg	Ka	52.5	6.9236	0.0202	0.0090	1.42	0.89	0.6369	5.61	A	1.36	1.48
Al	Ka	56.6	6.9236	0.0214	0.0096	1.34	0.76	0.7118	5.60	A	1.29	1.40
Si	Ka	135.7	6.9236	0.0537	0.0240	3.01	1.63	0.7979	10.65	A	2.93	3.08
S	Ka	15.8	3.6495	0.0080	0.0036	0.42	0.20	0.8615	3.21	B	0.38	0.45
Cl	Ka	47.7	3.6495	0.0268	0.0210	1.42	0.61	0.8459	5.74	A	1.35	1.48
K	Ka	161.3	3.6495	0.1103	0.0493	5.67	2.21	0.8686	16.48	A	5.54	5.81
Ca	Ka	213.6	3.6495	0.1630	0.0728	8.48	3.22	0.8582	23.84	A	8.31	8.66
Fe	Ka	5.2	0.2706	0.0098	0.0044	0.57	0.15	0.7685	2.81	B	0.49	0.64

Table 3
Estimation of different isotherm constants and correlation coefficients for the adsorption of MP and PP dyes onto ALLC AgNPs

Isotherm	Equation	Parameters	Value of parameters for PP dye	Value of parameters for MP dye
Langmuir	$q_e = \frac{q_m b C_e}{(1 + bC_e)}$	q_m (mg/g)	8.5	6.7
		K_L (L/mg)	0.19	0.43
		R^2	0.9742	0.9679
Freundlich	$\ln q_e = \ln K_F + \left(\frac{1}{n}\right)\ln C_e$	n	0.58	0.38
		K_F (mg)$^{1-n}$/L^n/g	1.9	2.4
		R^2	0.8948	0.7769
Temkin	$\log\left(\frac{1}{q_e}\right) = \log\left(\frac{k_L + 1}{k_L q_m}\right) + \frac{1}{n}\log\frac{1}{C_e}$	A_T (L/mg)	1.06	1.04
		B_T	10.346	21.2
		R^2	0.8706	0.6071

their surfaces. Unfortunately, it is experimentally difficult to measure the charges on the surface directly. Instead, indirect methods are available such as estimation of point of zero charge (PZC) from electrochemical impedance spectroscopy measurement. PZC is an expedient marker of surface charges that is critically relevant to the adsorption of an electrolyte [26]. It shows the potential when the surface carries zero charges. Normally, when electrode potential is larger than PZC, the electrode carries positive charges, and when it is smaller than PZC, the electrode carries negative charges. The solution's pH value affects the surface charge of the adsorbent, the uptake behavior, and the efficiency of

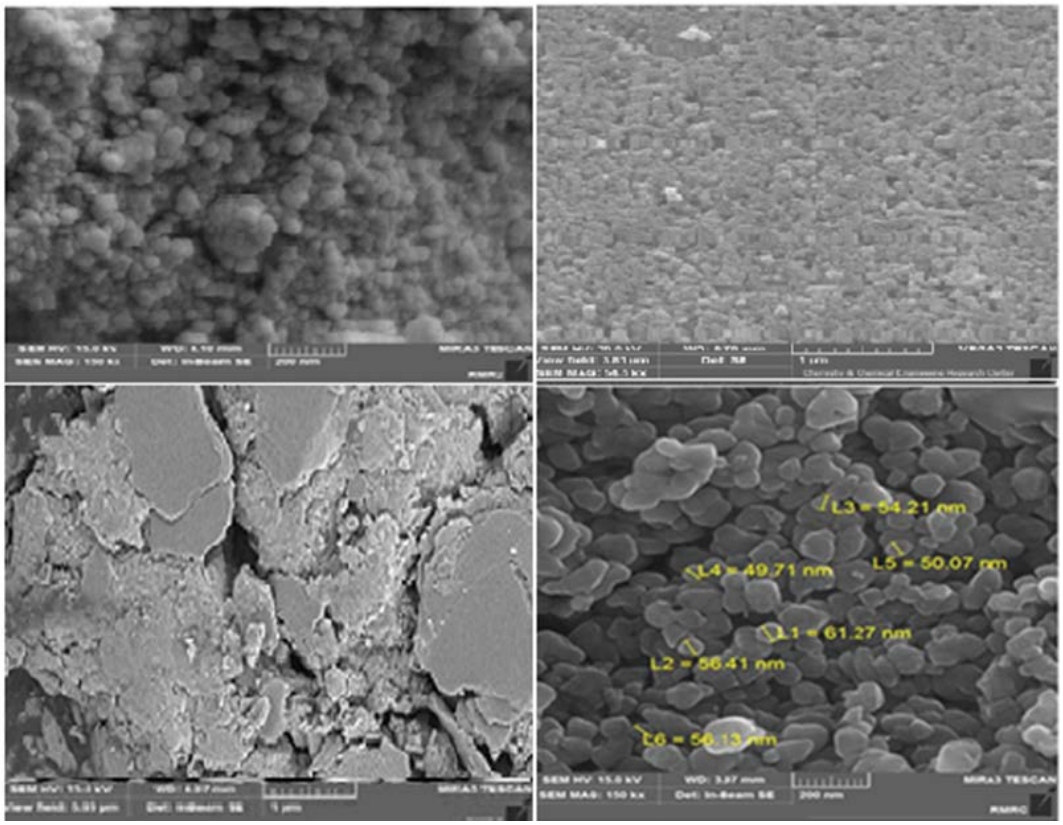

Fig. 6. SEM images of the ALLC AgNPs.

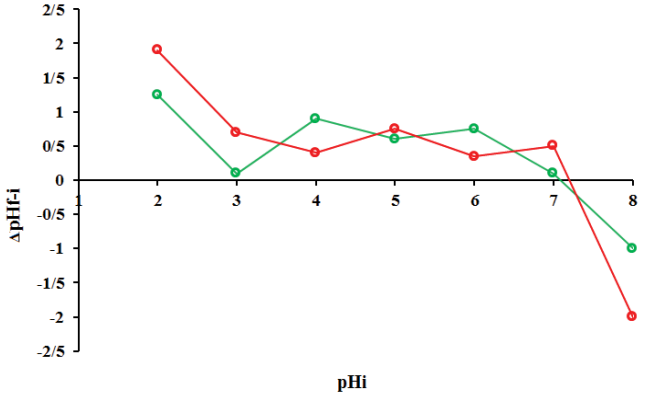

Fig. 7. pH_{PZC} of MP and PP dyes for adsorption onto sorption ALLC AgNPs.

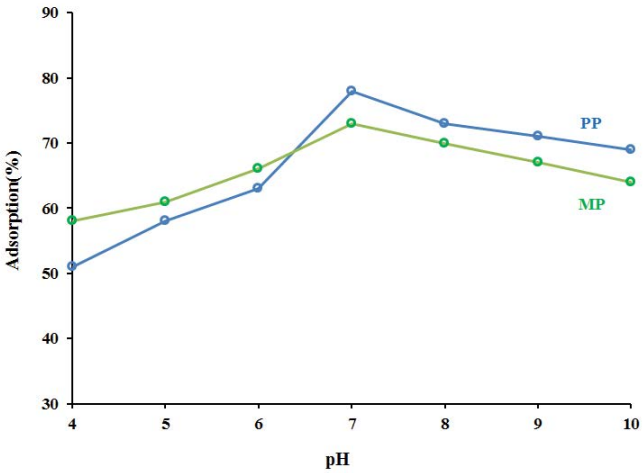

Fig. 8. Impact of pH on MP and PP dyes removal (paraben dyes conc.: 10 mg/L; contact time: 60 min; adsorbent dose: 50 mg; stirring speed: 180 rpm; temp.: 25°C).

the adsorbent. The difference between the initial and final pH values ($pH_f - pH_i$) was plotted against the pH was noted as the pH in which the initial pH and the final pH are equal (Fig. 7) [5,26].

3.2. *Effect of pH on the adsorption ΔpH*

The impact of pH value was investigated on the adsorption process of MP and PP dyes (Fig. 8). The adsorption amount of dyes with the initial concentrations of 10 mg/L was measured in the various pH ranges from 4 to 10 in the presence of the constant amount of adsorbent [27]. ALLC AgNPs provided the highest removal percentages of MP and PP dyes at pH 7.0, which were 73.3% for MP, and 78.4% for PP. Any decrease in dye removal at acidic pH (pH < 7) is due to MP and PP dyes' competition with H^+. However, in a highly acidic medium, protonation of nitrogen atoms occured on the adsorbent surface, which subsequently reduced interactions with parabens dyes. The decrease

in MP and PP dyes removal at pH > 7 can be related to the precipitation of MP, and PP dyes in the hydroxide form. Due to this phenomenon, the availability of paraben dyes to the adsorption sites is blocked, and as a result, less adsorption of MP and PP dyes occurs [28].

3.3. Effect of the adsorbent dosage

The dosage of adsorbent is known as a significant factor in the elimination of dyes. It is related to the adsorption capacity for the known concentration of dyes. Therefore, the adsorption efficiency for MP and PP dyes was investigated as a dose of the adsorbent. The percentage of dye adsorption increases sharply when the adsorbent is charged to 50 mg, as it is seen in Fig. 9.

This finding shows that when the adsorption sites are not yet saturated at the time of the adsorption process, the availability of adsorption sites was increased by increasing the dose of adsorbent [29]. Therefore, 50 mg was selected as the preferred dose of the adsorbent for subsequent experiments due to the highest absorption capacity.

This fact can be explained in another way that the small adsorbent ratio creates less active sites for dyes bind on the surface of ALLC AgNPs, and therefore, the sorption efficiency is low. Following the increase in sorbent dose, more active sites are provided, which increases adsorption efficiency until saturation.

3.4. Impact of contact time

Fig. 10 indicates the contact time influence on MP and PP dyes' adsorption process using synthesized ALLC AgNPs. As shown, a slight large in the adsorption amount occurs until 60 min and then at times more than 60 min slowly leveled off, and no significant increase was observed, illustrating that adsorptive equilibrium was achieved [30]. The percentages of 79.0% and 73.5% were recorded as the highest removal percentages for MP and PP dyes at contact time 60 min.

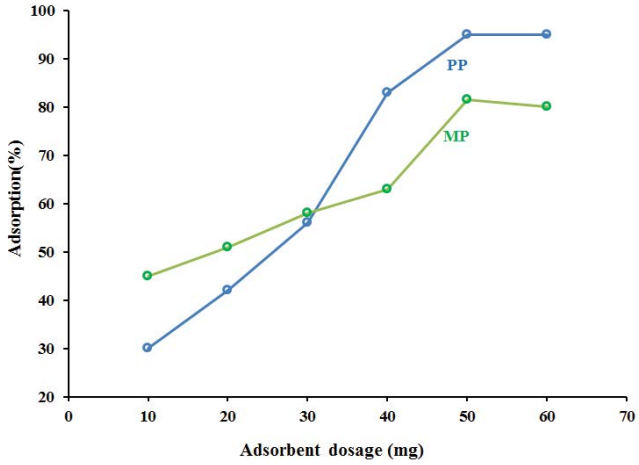

Fig. 9. Impact of the dosage of adsorbent on MP and PP dyes removal (paraben dyes conc.: 10 mg/L; pH: 7.0; stirring speed: 180 rpm; contact time: 60 min; temp.: 25°C).

3.5. Impact of temperature

Fig. 11 shows the influence of temperature on the adsorption process of MP and PP dyes on ALLC AgNPs. There is a gradual increase from 60.0% to 80.0% in the adsorption of MP and from 68.0% to 87.0% for PP. The preceding outcomes proved the endothermicity of the adsorption. Due to the feature and type of the adsorbent porosity and the probability of diffusion, the amount of adsorption enhanced with increasing temperature.

Furthermore, as the process is endothermic, the increase in temperature is favorite to dyes transport within the adsorbent pores [31].

3.6. Adsorption isotherms

The adsorbate molecules division among the solid and liquid phases in equilibrium is designated based on adsorption isotherms. Adsorption of MP and PP dyes onto ALLC AgNPs was modeled based on three adsorption isotherms of Freundlich, Langmuir, and Temkin [32] (Table 3).

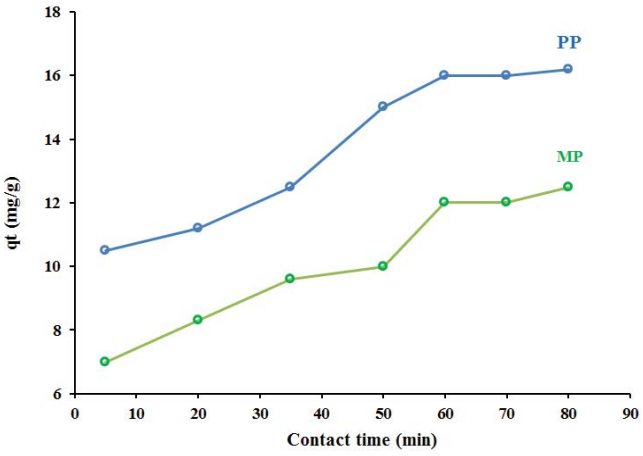

Fig. 10. Impact of time on MP and PP dyes removal (paraben dyes conc.: 10 mg/L; pH: 7.0; contact dose adsorbent: 50 mg; temp.: 25°C; stirring speed: 180 rpm).

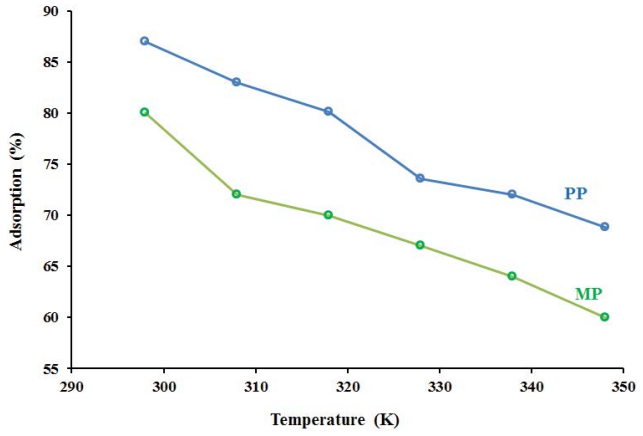

Fig. 11. Impact of temperature on MP and PP dyes removal (paraben dyes conc.: 10 mg/L; adsorbent dose: 50 mg; pH: 7.0; stirring speed: 180 rpm; contact time: 60 min).

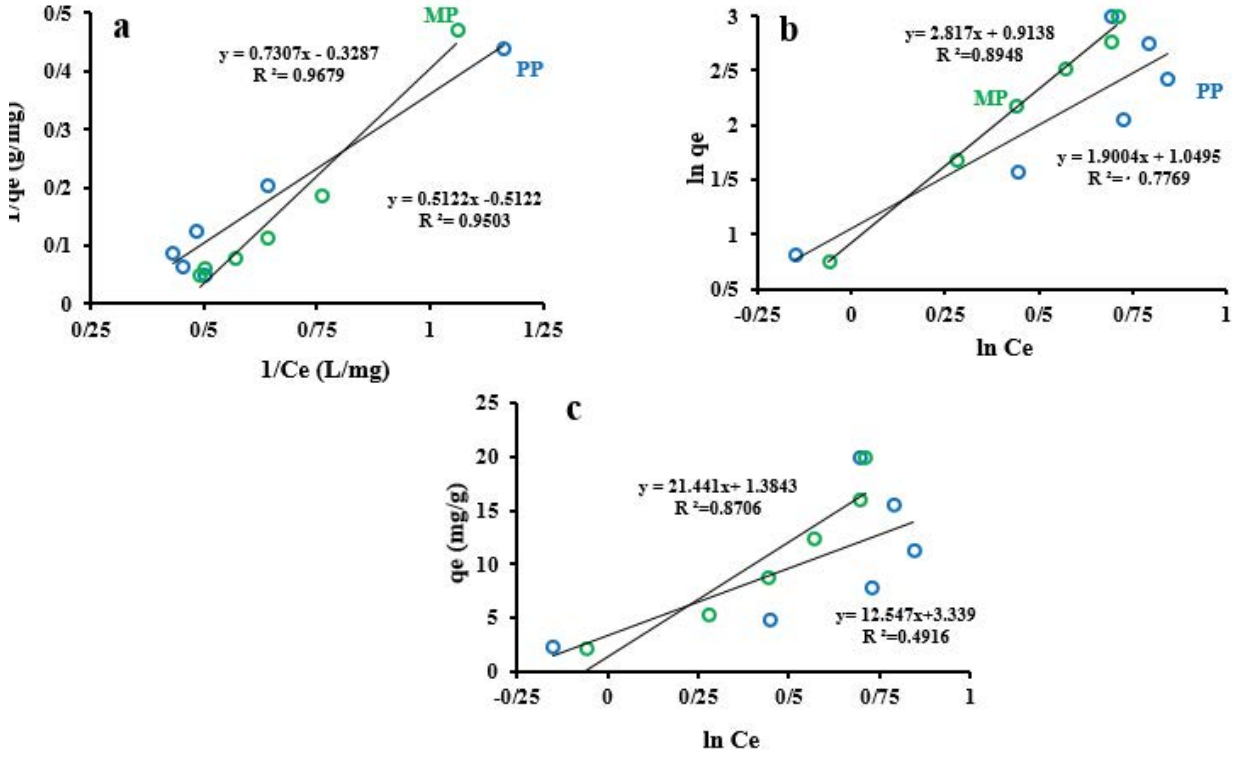

Fig. 12. (a) Langmuir, (b) Freundlich, and (c) Temkin isotherm for the adsorption of MP and PP dyes (initial paraben dyes conc.: 10 mg/L; pH: 7.0; adsorbents dose: 50 mg; temp.: 25°C).

A detailed description of adsorption isotherm at equilibrium state is possible based on the mathematical relevance between the (q_e) as mg/g and non-adsorbed quantity of dyes (C_e) as mg/L at the determined temperature [33,34]. For the accurate study of adsorption isotherms, the Langmuir, Freundlich, and Temkin models were employed (Fig. 12).

Based on the Langmuir model, there is no interaction between the adsorbed molecules and the adsorption process at homogeneous surfaces. The following equation presents the Langmuir model [35]:

$$\frac{C_e}{q_e} = \frac{1}{K_L q_{\max}} + \frac{C_e}{q_{\max}} \tag{3}$$

In the above equation C_e, q_e, q_{max}, and K_L are equilibrium concentration (mg/L), adsorption capacity (mg/g), and maximum of adsorption capacity (mg/g) and Langmuir constant (L/mg). The Langmuir model proved to be the best because it provides a strong correlation in all adsorbent masses. Increasing the amount of adsorbent caused a considerable increase in the adsorbed dyes amounts (Fig. 12a). Calculation of K_F and adsorption capacity in the Freundlich model was performed from the interception and slope of the linear plot of $\ln q_e$ vs. $\ln C_e$ (Fig. 12b) [36].

Temkin's isotherm model (Fig. 12c) was employed to evaluate adsorption heat and interaction between adsorbent and adsorbate based on the following equation:

$$q_e = \frac{Rt}{b}\ln K_T + \frac{RT}{b}\ln C_e \tag{4}$$

In this model, as mentioned above, R, b, t, K_T, and T are the universal gas constant (8.314 J/mol K), Temkin constant, the heat of the adsorption (J/mol), the binding constant at equilibrium (L/mg) and absolute temperature (K) [37].

The experimental data were fitted using these models. Considering the large values of correlation coefficient obtained for MP and PP dyes (R^2 = 0.98–0.97), it was confirmed the Langmuir model is the finest isotherm model for dyes adsorption explanation on ALLC AgNPs. The Langmuir isotherm depicts an adsorbent monolayer's creation on the outer adsorbent (ALLC AgNPs) surface quantitatively. It also indicates the equilibrium distribution of MP and PP dyes between the solid and liquid phases.

3.7. Adsorption kinetic study

Various parameters such as the solid-state (mostly with the non-uniform reactive surface) and chemical and physical states in which the adsorption took place can strongly influence the solute adsorption using an adsorbent in the aqueous solution via complicated stages [38]. The adsorption rates of dyes on the surface of the adsorbent were conformed to conventional kinetic models, including pseudo-first-order, pseudo-second-order, and Elovich models (Fig. 13). The kinetic data of adsorption were perfectly explained based on the pseudo-first-order model [39]. The following equation represents the Lagergren:

$$\frac{dq_t}{dt} = k_1\left(q_e - q_t\right) \tag{5}$$

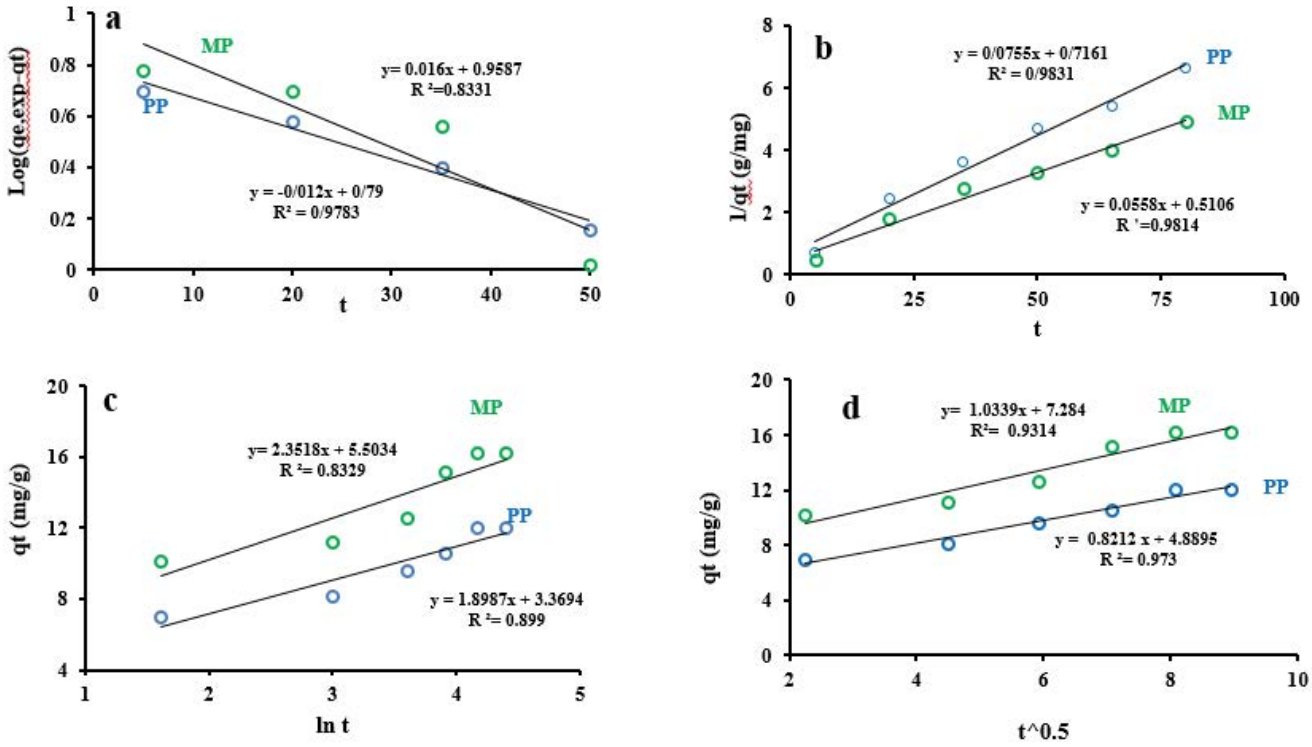

Fig. 13. (a) Pseudo-first-order, (b) pseudo-second-order, (c) intraparticle diffusion, and (d) Elovich model for MP and PP dyes adsorption (initial paraben dyes conc.: 10 mg/L; contact time: 60 min).

where q_e, q_t, k_1 are the equilibrium adsorption capacities (mg/g), adsorption capacities at any time (mg/g), and the rate constant of the pseudo-first-order adsorption (L/min). By plotting the $\log(q_e - q_t)$ against t, the values of q_e and k_1 were obtained using the line's intercept and slope, respectively.

$$\log\left(q_e - q_t\right) = \log q_t - \frac{k_1}{2.303}t \tag{6}$$

Since interception is not equal to q_e, it was proved that the action could not be the first-order (Fig. 13a).

When diffusion to the pore restricts the process of adsorption, a linear relationship between the initial concentration of solute and adsorption rate is detected. Therefore, the need to fit the empirical results with other kinetic models became apparent (Table 4).

Consequently, pseudo-second-order kinetic model [40] was introduced by Eq. (7):

$$\frac{dq_t}{dt} = k_2\left(q_e - q_t\right)^2 \tag{7}$$

For the interval 0 to t for t and 0 to q_t for q_t Eq. (6) was integrated to provide:

$$\frac{t}{q_t} = \frac{1}{k_2 q_e^2} + \frac{t}{q_e} \tag{8}$$

The perfect outcomes indicated that the entire adsorption period didn't match with the plot of $\log(q_e - q_t)$ vs. t, while the plot of t/q_t against t demonstrated a direct line (Fig. 13b). The q_e and k_2 values were calculated using the slope and intercept of the plot of t/q_t against t (Table 4). The estimated q_e values' similarities under several situations like different initial dye concentrations and/or adsorbent mass to the experimental data were observed.

Also, the suitability of this model for explanation of experimental data was confirmed from higher values of R^2.

Accordingly, the pseudo-second-order model was chosen for the whole adsorption period of MP and PP dyes. The following equation is the intraparticle diffusion equation [41]:

$$q_t = k_{\text{dif}} t^{1/2} + C \tag{9}$$

In this formula, the intraparticle diffusion rate constant and the boundary layer thickness in Fig. 13c were introduced as k_{dif} (mg/(g min$^{1/2}$) and C, respectively. The linear form of the Elovich model (Fig. 13d) is indicated as [42]:

$$q_t = \frac{1}{\beta}\ln\left(\alpha\beta\right) + \frac{1}{\beta}\ln t \tag{10}$$

In Table 4, the intraparticle diffusion and Elovich model, as well as the kinetic data from pseudo-first and pseudo-second-order adsorption kinetic models, are demonstrated. For different initial dyes concentrations, a favorable correlation was shown between experimental and estimated q_e values by the linear plots of t/q_t against t. Moreover, greater correlation coefficients of the pseudo-second-order kinetic model (R^2 = 0.9831, R^2 = 0.9891) than pseudo-first-order

Table 4
Comparison of the kinetic parameters for the removal of MP and PP dyes into ALLC AgNPs

Model	Parameters	Value of parameters for PP dye	Value of parameters for MP dye
Pseudo-first-order kinetic $\log(q_e - q_t) = \log(q_e) - \frac{k_1}{2.303}t$	$q_{e,cal}$ (mg/g)	46.5	30.5
	k_1 (min^{-1})	0.28	0.39
	R^2	0.9783	0.8676
Pseudo-second-order kinetic $\frac{t}{q_t} = \frac{1}{k_2 q_e^2} + \left(\frac{1}{q_e}\right)t$	$q_{e,cal}$ (mg/g)	78.4	88.0
	k_2 (g/mg min)	39.0	28.55
	R^2	0.9831	0.9814
Intraparticle diffusion $q_t = k_{intra}(t)^{1/2} + C$	K_i ((mg/g) min$^{-0.5}$)	0.812	1.00
	C (Å)	4.236	6.884
	R^2	0.899	0.8329
Elovich $q_t = \frac{1}{\beta}\ln(\alpha\beta) + \frac{1}{\beta}\ln(t)$	α (g/mg min)	10.62	23.12
	β (g/mg)	0.51	0.415
	R^2	0.973	0.9314

model (R^2 = 0.8676, R^2 = 0.99783), respectively for MP and PP dyes proved that the adsorption fit the pseudo-second-order better than the pseudo-first-order kinetic model.

3.8. Adsorption equilibrium investigation

For the adsorption processes, the thermodynamic parameters of changes of Gibbs free energy, enthalpy, and entropy $\Delta G°$, $\Delta H°$ and $\Delta S°$, respectively were considered. Their computation becomes possible through utilizing the following equations [43]:

$$K_c = \frac{C_A}{C_S} \tag{11}$$

$$\Delta G° = -RT\ln K_{ad} \tag{12}$$

$$\ln K_{ad} \frac{\Delta H°}{RT} + \frac{\Delta S°}{R} \tag{13}$$

From a graph based on lnK_e vs. 1/T as shown in Fig. 14, is provided. By considering the slope of this graph, $\Delta G°$ can be acquired. In Table 5, the summary of the thermodynamic parameter outcomes for MP and PP dyes adsorption on ALLC AgNPs at diverse temperatures is demonstrated.

The estimation of $\Delta G°$ values became possible via employing the equation adsorption of paraben dyes. According to Fig. 14, by increasing temperature from 298 to 348 K, a steep reduction in the ALLC AgNPs nanoparticles adsorbent was observed, which corroborates the exothermicity type of the adsorption process. The thermodynamic parameters (Table 5) [44], were computed using the plots. Moreover, the $\Delta G°$ with negative value supports the possibility and spontaneity nature of the adsorption process. On the other hand, the $\Delta H°$ with negative value strongly affirms the exothermicity type of the process, and the $\Delta S°$ value affirms an alteration in the unpredictability at the interface of ALLC AgNPs

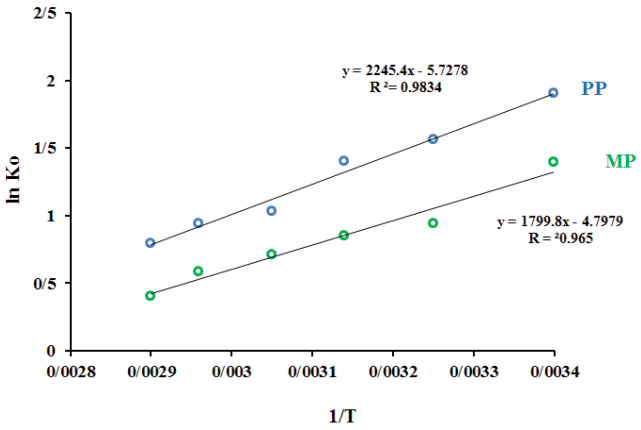

Fig. 14. The plot of lnK_c vs. 1/T for the estimation of thermodynamic parameters.

and solution. The conformity of $\Delta G°$ values up to –40.0 and –47.6 kJ/mol for MP and PP dyes with those of electrostatic interaction between adsorption sites and the MP and PP dyes (physical adsorption) has been documented. In this present work, the predominance of the physical adsorption mechanism in the adsorption process has been confirmed by the obtained $\Delta G°$ values for paraben dyes (<–5 kJ/mol) [45].

3.9. Adsorption mechanism of MP and PP dyes

The physical and chemical characteristics of ALLC AgNPs were substantially changed by calcination. The specific surface area and the amount of polar functional groups increased, and the adsorption performance improved. Overall, the adsorption mechanisms of MP and PP dyes on ALLC AgNPs were mainly attributed to two aspects: chemical adsorption and physical adsorption. Under acidic conditions, chemical adsorption is dominant. The carboxyls of MP and PP dyes undergo ion and/or proton exchange reactions with the reactive sites of ALLC AgNPs with hydroxyl groups. Hydroxyl groups on the adsorbent combine with

Table 5
Thermodynamic parameters for the adsorption of MP and PP dyes onto ALLC AgNPs adsorbent

Paraben dyes (mg/L)	T (K)	K_c	Value of $\Delta S°$ (J/mol K)	Value of $\Delta H°$ (kJ/mol)	Value of $\Delta G°$ (kJ/mol)
PP dye	298	6.7	–47.6	–18.7	–4.71
	308	4.5			–4
	318	4.03			–3.7
	328	2.79			–2.81
	338	2.57			–2.64
	348	2.21			–2.29
MP dye	298	4	–40.0	–15.0	–3.44
	308	2.6			–2.4
	318	2.33			–2.25
	328	2.03			–1.94
	338	1.87			–1.63
	348	1.5			–1.16

Table 6
Comparison of the amount of MP and PP dyes removed by different adsorbents

Dyes	Adsorbent	Adsorption capacity (mg/g)		References
		MP	PP	
MP and PP dyes	Magnetic waste tyre activated carbon-chitosan	85.9	90.0	[5]
MP and PP dyes	TiO_2NPs-AC	–	12.0	[6]
MP and PP dyes	β-cyclodextrin hexamethylene diisocyanate	0.0305	0.1854	[47]
MP and PP dyes	β-cyclodextrin toluene-2,6-diisocyanate	0.1019	0.2551	[47]
MP and PP dyes	Ionic liquids loaded onto the surface of a polymeric adsorbent grafted with modified magnetic nanoparticles	–	18.48	[48]
MP and PP dyes	Activated carbon based on coconut	7.52	–	[49]
MP and PP dyes	*Albizia lebbeck* leaves-AgNPs	6.7	8.5	Present study

H^+ in solution, thus resulting in a greater hydroxyl group exchange and the formation of ($–OH_2^+$), according to Eq. (A). Furthermore, proton exchange reactions occur between $–OH_2^+$ and the hydroxyl group with outer complexes Eqs. (B) and (C). Finally, the inner complex is formed by ligand exchange, according to Eqs. (D) and (E).

$$\text{AgNPs-ALLC} - \text{OH} + \text{H}^+ \rightarrow \text{AgNPs-ALLC} - \text{OH}_2^+ \quad \text{(A)}$$

$$\text{AgNPs-ALLC} - \text{OH}_2^+ + \text{MP} - \text{C(O)O}^- \leftrightarrow \text{AR} - \text{OH}_2^+\text{O}^- - \text{C(O)} - \text{MP} \quad \text{(B)}$$

$$\text{AgNPs-ALLC} - \text{OH}_2^+ + \text{PP} - \text{C(O)O}^- \leftrightarrow \text{AR} - \text{OH}_2^+\text{O}^- - \text{C(O)} - \text{PP} \quad \text{(C)}$$

$$\text{AgNPs-ALLC} - \text{OH}_2^+\text{O}^- - \text{C(O)} - \text{MP} \leftrightarrow \text{AgNPs-ALLC} - \text{OC(O)} - \text{MP} + \text{H}_2\text{O} \quad \text{(D)}$$

$$\text{AgNPs-ALLC} - \text{OH}_2^+\text{O}^- - \text{C(O)} - \text{PP} \leftrightarrow \text{AgNPs-ALLC} - \text{OC(O)} - \text{PP} + \text{H}_2\text{O} \quad \text{(E)}$$

In neutral and weak alkaline conditions, MP and PP dyes exhibit substantial proton loss and exist as free ions in solution, thus inhibiting the chemical adsorption to some extent. However, the porous structure of ALLC AgNPs, especially after modification, tempers the negative effect via physical adsorption [46].

3.10. Comparison for the amount of MP and PP dyes removed with other adsorbents

Table 6 demonstrates the maximum adsorption capacities of varied adsorbents for the removal of MP dye and PP dyes comparatively. The type and density of active sites in adsorbents that are responsible for the adsorption of dyes from the solution result in the variation in (q_{max}) values. The table's outcomes clearly show that the sorption capacity of utilized ALLC AgNPs in the current study is significantly high. In general, morphology, particle size and distribution, and surface structure of this sorbent were effective in its successful outcomes.

4. Conclusion

The selection of ALLC AgNPs as an impressive, useful, and affordable adsorbent to the removal of MP and PP dyes from solutions was evaluated. The optimum values of the pH, dosage of adsorbent, MP, and PP dyes concentration, and contact time were found to be 7, 50 mg, 10 mg/L, and 60 min, respectively, for adsorption of MP and PP dyes into ALLC AgNPs. Studying the impact of various parameters revealed that percent of adsorption decreased when initial paraben dyes concentration increased, but when adsorbent dosage increased, percent adsorption enhanced. The amounts of q_m for MP and PP dyes into ALLC AgNPs were obtained to be 6.7 and 8.5 mg/g, respectively. Equilibrium adsorption showed that the system followed the Langmuir model. The kinetics study indicated that MP and PP dyes removal complies based on the pseudo-second-order kinetic. Based on the regression-based linear analysis, it was found that the derived experimental models show an acceptable performance prediction to ALLC AgNPs with significant determination coefficients (R^2 = 0.994–0.984).

Also, the statistical results ensure that the recommended equations could favorably be used to adsorb MP and PP dyes from aqueous solutions.

Acknowledgment

The authors gratefully acknowledge the support of this work by Islamic Azad University, Branch of Omidiyeh Iran, for their partial support.

References

[1] M. Zubair, I. Ihsanullah, N. Jarrah, A. Khalid, M.S. Manzar, T.S. Kazeem, M.A. Al-Harthi, Starch-NiFe-layered double hydroxide composites: efficient removal of methyl orange from aqueous phase, J. Mol. Liq., 249 (2018) 254–264.
[2] I. Ihsanullah, A. Jamal, M. Ilyas, M. Zubair, G. Khan, M.A. Atieh, Bioremediation of dyes: current status and prospects, J. Water Process. Eng., 38 (2020) 101680, doi: 10.1016/j.jwpe.2020.101680.
[3] M.G. Soni, I.G. Carabin, G.A. Burdock, Safety assessment of esters of p-hydroxybenzoic acid (parabens), Food Chem. Toxicol., 43 (2005) 985–1015.
[4] P.D. Darbre, A. Aljarrah, W.R. Miller, N.G. Coldham, M.J. Sauer, G.S. Pope, Concentrations of Parabens in human breast tumours, J. Appl. Toxicol., 24 (2004) 5–13.
[5] G.P. Mashile, A. Mpupa, A. Nqombolo, K.M. Dimpe, P.N. Nomngongo, Recyclable magnetic waste tyre activated carbon-chitosan composite as an effective adsorbent rapid and simultaneous removal of methylparaben and propylparaben from aqueous solution and wastewater, J. Water Process Eng., 33 (2020) 101011, doi: 10.1016/j.jwpe.2019.101011.
[6] M. Pargari, F. Marahel, B. Mombini Godajdar, Ultrasonic assisted adsorption of propylparaben on uultrasonically synthesized TiO_2 nano particles loaded on activated carbon: optimization, kinetic and equilibrium studies, Desal. Water Treat., 103 (2018) 248–260.
[7] S. Ito, S. Yazawa, Y. Nakagawa, Y. Sasaki, S. Yajima, Effects of alkyl parabens on plant pathogenic fungi, Bioorg. Med. Chem. Lett., 25 (2015) 1774–1777.
[8] J.R. Byford, L.E. Shaw, M.G.B. Drew, G.S. Pope, M.J. Sauer, P.D. Darbre, Oestrogenic activity of parabens in MCF7 human breast cancer cells, J. Steroid Biochem. Mol. Biol., 80 (2002) 49–60.
[9] L. Dewalque, C. Pirard, C. Charlier, Measurement of urinary biomarkers of parabens, benzophenone-3, and phthalates in a Belgian population, Biomed Res. Int, 2014 (2014), doi: 10.1155/2014/649314.
[10] S. Oishi, Effects of propylparaben on the male reproductive system, Food Chem. Toxicol., 40 (2002) 1807–1813.
[11] J.F. Gomes, I. Leal, K. Bednarczyk, M. Gmurek, M. Stelmachowski, M. Diak, M. Emília Quinta-Ferreira, R. Costa, R.M. Quinta-Ferreira, R.C. Martins, Photocatalytic ozonation using doped TiO_2 catalysts for the removal of parabens in water, Sci. Total Environ., 609 (2017) 329–340.
[12] P. Canosa, I. Rodríguez, E. Rubí, M.H. Bollaín, R. Cela, Optimisation of a solid-phase microextraction method for the determination of parabens in water samples at the low ng per litre level, J. Chromatogr. A, 1124 (2006) 3–10.
[13] L. Núñez, J.L. Tadeo, A.I. García-Valcárcel, E. Turiel, Determination of parabens in environmental solid samples by ultrasonic-assisted extraction and liquid chromatography with triple quadrupole mass spectrometry, J. Chromatogr. A, 1214 (2008) 178–182.
[14] M. Díaz-Álvarez, S.P. Smith, D.A. Spivak, A. Martín-Esteban, Preparation of molecularly imprinted polymeric fibers using a single bifunctional monomer for the solid-phase microextraction of parabens from environmental solid samples, J. Sep. Sci., 39 (2016) 552–558.
[15] J. Abdi, M. Vossoughi, N.M. Mahmoodi, I. Alemzadeh, Synthesis of metal-organic framework hybrid nanocomposites based on GO and CNT with high adsorption capacity for dye removal, Chem. Eng. J., 326 (2017) 1145–1158.
[16] S.J.P. Jacob, J.S. Finub, A. Narayanan, Synthesis of silver nanoparticles using Piper longum leaf extracts and its cytotoxic activity against Hep-2 cell line, Colloids Surf., B, 91 (2012) 212–214.
[17] C. Han, L. Zhang, H. Li, Highly selective and sensitive colorimetric probes for Yb^{3+} ions based on supramolecular aggregates assembled from β-cyclodextrin-4,4′-dipyridine inclusion complex modified silver nanoparticles, Chem. Commun., 24 (2009) 3545–3547.
[18] F.J. Heiligtag, M. Niederberger, The fascinating world of nanoparticle research, Mater. Today, 16 (2013) 262–271.
[19] V.V. Kumar, S. Anbarasan, L.R. Christena, N. Saisubramanian, S. Philip Anthony, Bio-functionalized silver nanoparticles for selective colorimetric sensing of toxic metal ions and antimicrobial studies, Spectrochim. Acta, Part A, 129 (2014) 35–42.
[20] A. Dias, V.S.T. Ciminelli, Analysis of nitrogen adsorption-desorption isotherms for the estimation of pore-network dimensions and structure of ferroelectric powders, Ferroelectrics, 247 (2000) 9–16.
[21] A. Dehghanpoor Frashah, S. Hashemian, F. Tamadon, Ag doped hydroxyapatite nano particles for removal of methyl red azo dye from aqueous solutions kinetic and thermodynamic studies, Eur. J. Anal. Chem., 15 (2020) 32–44.
[22] T. Graf, F. Casper, J. Winterlik, B. Balke, H. Gerhard, C. Felser, T. Graf, F. Casper, J. Winterlik, B. Balke, G.H. Fecher, Crystal structure of New Heusler compounds, J. Inorg. Gen. Chem., 635 (2009) 976–981.
[23] N. Bobby, W. Eg, M. Johnson, FT-IR studies on the leaves of *Albizia lebbeck* benth, Int. J. Pharm. Pharm. Sci., 4 (2012) 293–296.
[24] M. Naushad, G. Sharma, Z.A. Alothman, Photodegradation of toxic dye using Gum Arabic-crosslinked-poly(acrylamide)/$Ni(OH)_2$/FeOOH nanocomposites hydrogel, J. Cleaner Prod., 241 (2019) 112863, doi: 10.1016/j.jclepro.2019.118263.
[25] M. Zahed, D. Jafari, M. Esfandyari, Adsorption of formaldehyde from aqueous solution using activated carbon prepared from *Hibiscus rosa-sinensis*, Int. J. Environ. Anal. Chem., (2020) 1762872, doi: 10.1080/03067319.
[26] E. Moawed, A. Abulkibash, M. El-Shahat, Synthesis and characterization of iodo polyurethane foam and its application in removing of aniline blue and crystal violet from laundry wastewater, J. Taibah Univ. Sci., 9 (2015) 80–88.

[27] M. Ghaedi, B. Sadeghian, A.A. Pebdani, R. Sahraei, A. Daneshfar, C. Duran, Kinetics, thermodynamics and equilibrium evaluation of direct yellow 12 removal by adsorption onto silver nanoparticles loaded activated carbon, Chem. Eng. J., 187 (2012) 133–141.
[28] B.C. da Silva, A. Zanutto, J.M.T.A. Pietrobelli, Biosorption of reactive yellow dye by malt bagasse, Adsorpt. Sci. Technol., 37 (2019) 236–259.
[29] Q. Zhou, W. Gong, C. Xie, D. Yang, X. Ling, X. Yuan, S. Chen, X. Liu, Removal of neutral red from aqueous solution by adsorption on spent cottonseed hull substrate, J. Hazard. Mater., 185 (2011) 502–506.
[30] G. Absalan, A. Bananejad, M. Ghaemi, Removal of alizarin red and purpurin from aqueous solutions using $CoFe_2O_4$ magnetic nanoparticles, Anal. Bioanal. Chem. Res., 99 (2008) 65–77.
[31] S. Hajati, M. Ghaedi, B. Barazesh, F. Karimi, R. Sahraei, A. Daneshfar, A. Asghari, Application of high order derivative spectrophotometry to resolve the spectra overlap between BG and MB for the simultaneous determination of them: ruthenium nanoparticle loaded activated carbon as adsorbent, J. Ind. Eng. Chem., 20 (2014) 2421–2427.
[32] M. Arabi, A. Ostovan, A.R. Bagheri, X. Guo, J. Li, J. Ma, L. Chen, Hydrophilic molecularly imprinted nanospheres for the extraction of rhodamine B followed by HPLC analysis: a green approach and hazardous waste elimination, Talanta, 215 (2020) 120933, doi: 10.1016/j.talanta.2020.120933.
[33] G. Haghdoost, Removal of Reactive Red 120 from aqueous solutions using *Albizia lebbeck* fruit (pod) partical as a low cost adsorbent, J. Phys. Theor. Chem., 15 (2019) 141–148.
[34] S. Hajati, M. Ghaedi, H. Mazaheri, Removal of methylene blue from aqueous solution by walnut carbon: optimization using response surface methodology, Desal. Water Treat., 57 (2016) 3179–3193.
[35] I. Langmuir, The adsorption of gases on plane surfaces of glass, mica and platinum, J. Am. Chem. Soc., 40 (1918) 1361–1403.
[36] H.M.F. Freundlich, Over the adsorption in solution, J. Phys. Chem. A, 57 (1906) 385–470.
[37] M. Temkin, Adsorption equilibrium on hetrogeneous surfaces, J. Phys. Chem., 20 (1964) 1441.
[38] T.K. Kim, T. Kim, W.S. Choe, M.K. Kim, Y.J. Jung, K.D. Zoh, Removal of heavy metals in electroplating wastewater by powdered activated carbon (PAC) and sodium diethyldithiocarbamate-modified PAC, Environ. Eng. Res., 23 (2018) 301–308.
[39] Y.S. Ho, Review of second-order models for adsorption systems, J. Hazard. Mater., 136 (2006) 681–689.
[40] A.R. Bagheri, M. Ghaedi, A. Asfaram, A.A. Bazrafshan, R. Jannesar, Comparative study on ultrasonic assisted adsorption of dyes from single system onto Fe_3O_4 magnetite nanoparticles loaded on activated carbon: experimental design methodology, Ultrason. Sonochem., 34 (2017) 294–304.
[41] P. Senthil Kumar, K. Ramakrishnan, R. Gayathri, Removal of nickel(II) from aqueous solutions by ceralite IR 120 cationic exchange resins, J. Eng. Sci. Technol., 5 (2010) 234–245.
[42] M. Toor, B. Jin, Adsorption characteristics, isotherm, kinetics, and diffusion of modified natural bentonite for removing diazo dye, Chem. Eng. J., 187 (2012) 79–88.
[43] S. Falahrodbari, Adsorption of benzene butyl phthalate with mullti-walled carbon nanotubes/Ag nanoparticles and its applications, Orient. J. Chem., 33 (2017) 910–919.
[44] O.S. Bello, T.T. Siang, M.A. Ahmad, Adsorption of Remazol Brilliant Violet-5R reactive dye from aqueous solution by cocoa pod husk-based activated carbon: kinetic, equilibrium and thermodynamic studies, J. Chem. Eng., 12 (2011) 15–23.
[45] P. Senthil Kumar, S. Ramalingam, C. Senthamarai, M. Niranjanaa, P. Vijayalakshmi, S. Sivanesan, Adsorption of dye from aqueous solution by cashew nut shell: studies on equilibrium isotherm, kinetics and thermodynamics of interactions, Desalination, 261 (2010) 52–60.
[46] S. Mustapha, D.T. Shuaib, M.M. Ndamitso, M.B. Etsuyankpa, A. Sumaila, U.M. Mohammed M.B. Nasirudeen, Adsorption isotherm, kinetic and thermodynamic studies for the removal of Pb(II), Cd(II), Zn(II) and Cu(II) ions from aqueous solutions using *Albizia lebbeck* pods, Appl. Water Sci., 9 (2019) 142–153.
[47] Y.P. Chin, S. Mohamad, M.R. Bin Abas, Removal of parabens from aqueous solution using ß-cyclodextrin cross-linked polymer, Int. J. Mol. Sci., 11 (2010) 3459–3471.
[48] M. Md Yusoff, N. Yahaya, N.M. Saleh, M. Raoov, A study on the removal of propyl, butyl, and benzyl parabens via newly synthesised ionic liquid loaded magnetically confined polymeric mesoporous adsorbent, RSC Adv., 8 (2018) 25617–25635.
[49] P. Atheba, N. Guadi, B. Allou, P. Drogui, A. Trokourey, Adsorption kinetics and thermodynamics study of butylparaben on activated carbon coconut based, J. Encapsul. Adsorpt. Sci., 8 (2018) 39–57.